ISSN 1674-1056
http://cpb.iphy.ac.cn
http://iopscience.iop.org/cpb
中国物理 B
Chinese Physics
中国物理
Chinese Physics B

Fabrication of mixed perovskite organic cation thin films via controllable cation exchange

Yu-Long Zhao(赵宇龙), Jin-Feng Wang(王进峰), Ben-Guang Zhao(赵本广), Chen-Chen Jia(贾晨晨), Jun-Peng Mou(牟俊朋), Lei Zhu(朱磊), Jian Song(宋健), Xiu-Quan Gu(顾修全), Ying-Huai Qiang(强颖怀)
Citation: Chin. Phys. B . 2018, 27(2): 024208. **doi:** 10.1088/1674-1056/27/2/024208

Journal homepage: http://cpb.iphy.ac.cn; http://iopscience.iop.org/cpb

What follows is a list of articles you may be interested in

A new kind of superimposing morphology for enhancing the light scattering in thin film silicon solar cells：Combining random and periodic structure

Huang Zhen-Hua, Zhang Jian-Jun, Ni Jian, Wang Hao, Zhao Ying
Chin. Phys. B . 2014, 23(8): 084205. **doi:** 10.1088/1674-1056/23/8/084205

Novel wavelength-accurate InP-based arrayed waveguide grating

Pan Pan, An Jun-Ming, Wang Hong-Jie, Wang Yue, Zhang Jia-Shun, Wang Liang-Liang, Dai Hong-Qing, Zhang Xiao-Guang, Wu Yuan-Da, Hu Xiong-Wei
Chin. Phys. B . 2014, 23(4): 044210. **doi:** 10.1088/1674-1056/23/4/044210

Four distributed feedback laser array integrated with multimode-interference and semiconductor optical amplifier

Ma Li, Zhu Hong-Liang, Liang Song, Zhao Ling-Juan, Chen Ming-Hua
Chin. Phys. B . 2013, 22(5): 054211. **doi:** 10.1088/1674-1056/22/5/054211

Optical properties of the two-port resonant tunneling filters in two-dimensional photonic crystal slabs

Ren Cheng, Cheng Li-Feng, Kang Feng, Gan Lin, Zhang Dao-Zhong, Li Zhi-Yuan
Chin. Phys. B . 2012, 21(10): 104210. **doi:** 10.1088/1674-1056/21/10/104210

Fabrication of mixed perovskite organic cation thin films via controllable cation exchange*

Yu-Long Zhao(赵宇龙), Jin-Feng Wang(王进峰), Ben-Guang Zhao(赵本广), Chen-Chen Jia(贾晨晨), Jun-Peng Mou(牟俊朋), Lei Zhu(朱磊), Jian Song(宋健), Xiu-Quan Gu(顾修全), and Ying-Huai Qiang(强颖怀)†

School of Materials Science and Engineering, China University of Mining and Technology, Xuzhou 221116, *China*

(Received 8 July 2017; revised manuscript received 3 November 2017; published online 5 January 2018)

Here in this paper, we demonstrate a facile technique for creating the mixed formamidinium ($HN=CHNH_3^+$, FA^+) and methylammonium ($CH_3NH_3^+$, MA^+) cations in the lead iodide perovskite. This technique entails a facile drop-casting of formamidinium iodide (FAI) solutions on as-prepared $MAPbI_3$ perovskite thin films under the controlled conditions, which leads to controllable displacement of the MA^+ cations by FA^+ cations in the perovskite structure at room temperature. Uniform and controllable mixed organic cation perovskite thin films without a "bi-layered" or graded structure are achieved. By applying this approach to photovoltaic devices, we are able to improve the performances of devices through extending their optical-absorption onset further into the infrared region to enhance solar-light harvesting. Additionally, this work provides a simple and efficient technique to tune the structural, electrical, and optoelectronic properties of the light-harvesting materials for high-performance perovskite solar cells.

Keywords: organic–inorganic perovskitesolar cell, morphology, cation exchange, drop-casting

PACS: 42.82.Gw, 42.88.+h, 42.90.+m **DOI:** 10.1088/1674-1056/27/2/024208

1. Introduction

Hybrid organic–inorganic lead halide perovskite solar cells (PSCs) have recently attracted tremendous attention due to their meteoric rise in power conversion efficiency (PCE), rocketing from 3.8% to 22.1% up to now within a few years. The reason for this amazingly rapid increase in PCE of PSCs is that perovskite materials possess most of the properties required to be excellent absorbers: intense light harvesting, bipolar semiconductivity, small exciton binding energy, apparent tolerance of defects, and long charge carrier (hole and electron) diffusion length and lifetime.[1–3] Methylammonium lead triiodide ($MAPbI_3$) is the pioneering material and a vast array of processing methods have been developed, such as the solution method, vapor deposition, vapor-assisted solution process (VASP) method, and other derivative techniques.[4] The solution method of $MAPbI_3$ perovskite is usually followed by two methods: one is a two-step method,[5] i.e., spin coating PbI_2 and then deposit $CH_3NH_3I_3$, and the other is a one-step method, i.e., directly spin coating a mixture solution of CH_3 NH_3 I and PbI_2.[6]

Despite the great success, $MAPbI_3$ is still non-optimal in terms of optical absorption onset ($\sim$ 1.57 eV). There is growing interest in formamidinium lead triiodide ($FAPbI_3$) perovskite. Compared with $MAPbI_3$, $FAPbI_3$ has a small band gap ($\sim$ 1.45 eV) with redshifted absorption onset, to improve the light-harvesting efficiency and consequently the short circuit photocurrent density of the related photovoltaic devices. The unique crystal structure character of $FAPbI_3$ is attributed to the larger ion size of FA^+ than that of MA^+ (the ionic radii of FA^+ and MA^+ are 2.53 Å and 2.17 Å, respectively).[7–9] With band gap tuning, the perovskite charge transport property becomes a fundamental ingredient of a working device with efficient electron and hole transport representing a stringent requirement in solar cells.

However, the preparation of the high-quality $FAPbI_3$ perovskite film is still a challenge, which is associated with the following factors. First, the "ionic radius" and symmetries of FA^+ and MA^+ cations are quite different, both of which are deemed to affect the growth dynamics of $FAPbI_3$ perovskite. Second, $FAPbI_3$ also crystallizes into a yellow δ-$FAPbI_3$ non-perovskite polymorph phase, as a byproduct, which is not easy to fully transform into α-$FAPbI_3$ when it fills the scaffold layer probably because of the stress from the substrate. Cation exchange may be an efficient method of fabricating high-quality pure α-$FAPbI_3$, which is most often used to retain the initial structure of a material whilst changing the composition.The ion-exchange reaction of $MAPbI_3 + FA^+ \leftrightarrow FAPbI_3 + MA^+$ may be a possible strategy for the phase conversion.

A few attempts have been made to fabricate α-$FAPbI_3$ perovskite based on cation exchange. For example, Zhou *et al.* reported a simple exposure of $MAPbI_3$ perovskite thin films to FA gas at 150 °C, leading to the rapid displacement of the MA^+ cations by FA^+ cations in the perovskite structure. The resulting α-$FAPbI_3$ perovskite thin film preserves the microstructural morphology of the original $MAPbI_3$ thin film exceptionally well. But the structure of the resulting film is not

*Project supported by the Fundamental Research Funds for the Central Universities, China (Grant No. 2015QNA09).

†Corresponding author. E-mail: yhqiang@cumt.edu.cn

© 2018 Chinese Physical Society and IOP Publishing Ltd

optimal with an evident graded structure hindering the cells from efficiency improving.[10] Cui *et al.* presented an organic cation exchange method to directly grow α-$FAPbI_3$ perovskite films by using NH_4PbI_3 and FA-Ac as precursors through using the chemical vapor deposition (CVD) technique. The PCE of the champion device was 12.4% based on the mesoscopic structure with no hysteresis.[11] However, this technique requires expensive apparatus and a high vacuum, which is too energy consuming and hinders mass production. Pellet *et al.* reported a sequential deposition method and the addition of 20% MA to the FA dipping bath that completely avoided the undesirable formation of the δ-phase while maintaining the red-shifted band gap of pure $FAPbI_3$.[12] Snaith *et al.* also demonstrated a similar process by dipping films of $MAPbI_3$ in a solution of FAI and observed uniform conversion through the entirety of the bulk film.[13] Although their work represents significant advancement toward high-quality δ-phase perovskite, the "solution dipping" method is restricted in industrial applications, because it has lots of disadvantages, such as it is not easy to precisely control, wasting raw materials, etc.

Mixing precursor solution, one of the cheapest film production methods, is widely used in solution-processed $MA_{1-x}FA_xPbI_3$ perovskite solar cell. Recently, Chuang *et al.* prepared $MA_{1-x}FA_xPbI_{3-y}Br_y$ based on one-step method by regulating precursor components.[14] Jian *et al.* fabricated formamidinium based perovskite solar cells at low temperature and enhanced performance by adding methylammonium chloride into precursor solutions.[15] However, simple spin-coating did not yield a homogeneous perovskite layer having tiny pinholes on surface due to centrifugal force and evaporation of solvents.

Here, we demonstrate the use of the optimized solution chemistry technology instead of the "solution dipping" method for fabricating mixed perovskite organic cation thin film, which includes drop-casting and spin-coating (Fig. 1). The key step is to grow the mixed (MA, FA)PbI_3 film via an *in situ* reaction of the as-deposited film of $MAPbI_3$ with FAI. We use $MAPbI_3$ as a crystal seed to modulate the growth of $FAPbI_3$ crystal and form the high-quality mixed-cation perovskite layer $MA_{1-x}FA_xPbI_3$. The growth substrates of crystals differ from others reported in the literature.[16] We mainly investigate the optimal FAI concentration based on this drop-casting technology.

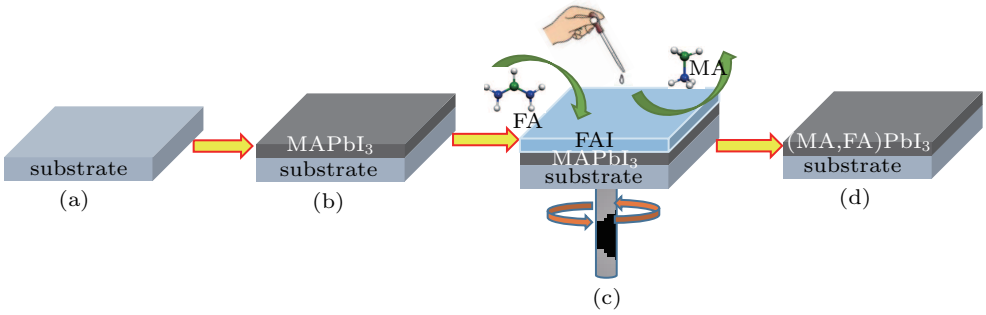


Fig. 1. (color online) Schematic illustration of perovskite film formation through drop-casting method.

2. Experimental details

2.1. CH_3NH_3I synthesis

CH_3NH_3I (MAI) was synthesized by mixing the CH_3NH_2 solution and the HI solution by 1:1 molar ratio in a round-bottom flask at 0 °C for 2 hours under stirring. The solvent was evaporated and the precipitate was washed with diethyl ether. The precipitate was dried at 60 °C for 24 hours in a vacuum oven.

2.2. Perovskite fabrication

Fluorine-doped tin oxide (FTO, Pilkington, TEC 15) glass substrate was partially etched with Zn powder and 2-M HCl to form the electrode pattern. Then, the substrate was cleaned with deionized water, ethanol, isopropanol, and absolute ethyl alcohol for 20 minutes, in sequence. A 50-nm-thick dense blocking TiO_2 was deposited via the spin-coated method, which was followed by a heating process at 450 °C for 30 minutes. The perovskite layer was deposited by using the one-step method reported in the literature.[17] The perovskite solutions were prepared by reacting the synthesized CH_3NH_3I powder (0.410 g) and $PbCl_2$ (Aldrich) (0.254 g) with a corresponding quantity of 1-ml *N*, *N*-Dimethylformamide (DMF) solvent. Then the mixture solution was agitated and heated for 2 hours at 75 °C in a glove box. The mixture solution was then coated onto the (cp) TiO_2/FTO substrate by spin coating at 2000 rpm for 60 seconds and dried on a hot plate at 60 °C for 10 minutes, 80 ° for 10 minutes, and 100 °C for 40 minutes, respectively. The FAI powder was obtained commercially from Sigma-Aldrich. The FAI power was dissolved in isopropanol solvent, and the solution concentrations were 2 mg/ml, 5 mg/ml, 10 mg/ml, and 15 mg/ml, respectively. Then these solutions were dropped onto the perovskite ($MAPbI_3$) layer, and after a 90-s reaction the reaction product was spin coated at 3000 rpm for 10 seconds and then dried on a hot plate at 150 °C for 15 minutes. The hole

transporting layer (HTL) was deposited by spining coating at 3000 rpm for 30 seconds. The HTL was synthesized by spiro-OMeTAD powder (72.3 mg) with additives of 17.5-μl Li-bis (trifluoromethanesulfonyl) imide (Li-TFSI), 28.8-μl 4-tert-butylpyridine (TBP), and 1-ml chlorobenzol. Finally, 50-nm-thick Ag was thermally evaporated on the top of the device to form the back contact. The active area of the device was 10 mm^2 determined by a black mask with dimensions of 2 mm×5 mm.

2.3. Characterization

The morphology, cross-sections, crystal structure and photoluminescence (PL) spectra of TiO_2/ $FA_xMA_{1-x}PbI_3$ films were characterized by a field emission scanning electron microscope (FESEM, S-4800, Hitachi, Japan), an x-ray diffraction (XRD, DX-2700B) and a steady state fluorescence spectrophotometer (Cary 300, Varian, USA) spectrometer, respectively. The UV-vis spectrophotometer (Cary 300, Varian, USA) was employed to characterize the diffusion absorption spectra. Photocurrent–voltage (J–V) curves of perovskite solar cells were characterized by a Keithley 2420 Source Meter under solar illumination (100 mW·cm^{-2}, Oriel Sol 3A, Newport) which was calibrated by a standard silicon solar cell (Oriel Instrument). The incident-photon-to-current conversion efficiency (IPCE) was measured by using a power source (Newport 300W Xenon lamp, 66902) with a monochromator (Newport Cornerstone 260) and a power meter (Newport 2936-C). The Fourier transform infrared spectroscopy (FTIR) spectrum (4000 cm^{-1}–500 cm^{-1}) was recorded on a Shimadzu UV 2550 spectrophotometer.

3. Results and discussion

The fabricated device includes FTO substrate, TiO_2 compact layer, perovskite ($FA_xMA_{1-x}PbI_3$) layer, spiro-OMeTAD hole transporting layer, and Ag electrode, respectively (shown in Fig. 2(a)). Besides, band-gap tuning of the perovskite hybrid can be flexibly modified via the substitution of MA^+ ions with FA^+ ions to optimize the absorbing layer (shown in Fig. 2(b)). According to the first principles calculations, both anions and molecular cations should have low activation energy for migration in the process of ionic conduction. The activation energies for I^- and MA^+ are 0.6 eV and 0.8 eV, respectively, which suggests that the cation exchange should be able to occur in a similar manner to the anion exchange.[13] It has been reported in the literature that the solid–liquid cation exchange reaction can be divided into two stages. One is the exchange of MA^+ with the FA^+ cation on the solid–liquid interface, and the other is cation migration of MA^+ and FA^+ in solid crystal.[18] Based on the above understanding of cation exchange reaction, a diffusion process of the FA^+ and MA^+ during annealing was schematically illustrated in Fig. 3. Both the interface exchange reaction and inner cation diffusion are mostly affected by ionic concentration and environmental temperature. Concentration of FAI solution is a key point to quickly forming uniform $FA_xMA_{1-x}PbI_3$ perovskite film because only a few hundred microliters of volume was used based on the "drop-casting" technique. The annealing temperature of $FA_xMA_{1-x}PbI_3$ perovskite film was 150 °C for 15 min according to the literature.[19] Nam–Gyu Park[19] demonstrated that the best performance can be obtained from the $FAPbI_3$ heated at 150 °C. High temperature can drastically increase the molecule moving speed (kinetic energy), while the high temperature will strongly deteriorate the film morphology due to the fast evaporation of isopropanol solvent. The reaction time was set to be 90 seconds in this "drop-casting" technology, because we found that crystallization has no significant change with the reaction time being longer. The x-ray diffraction spectra of $FA_xMA_{1-x}PbI_3$ film (10-mg/ml FAI) with different reaction times are shown in Fig. 4.

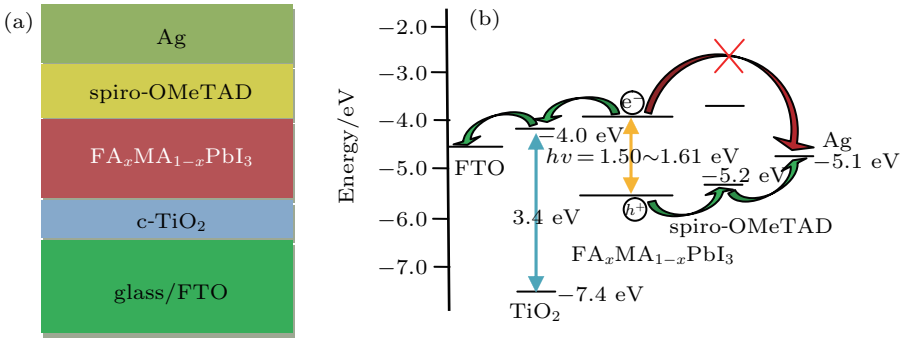


Fig. 2. (color online) (a) Schematic structure of the PSCs device based on $FA_xMA_{1-x}PbI_3$ perovskite film, and (b) energy level diagram for the corresponding material used in our device.

The x-ray diffraction (XRD) measurements were conducted to investigate crystal structure variations of the perovskite ($FA_xMA_{1-x}PbI_3$) films reacting with different concentrations of FAI solution. As shown in Fig. 5(a), all samples show the characteristic diffraction peaks of perovskite, which were verified by the dominant diffraction peaks at 14.2° and 28.5°, corresponding to the reflections from (110) and (220), respectively. In addition, the diffraction peak of PbI_2 was not

detected at $2\theta = 12.7°$, which means excellent crystallinity and a high level of phase purity of the perovskite film. In order to determine the optimal reaction concentration of FAI solution, figure 5(b) shows the XRD patterns monitored in the 2θ range of 28°–29° with increasing concentration. Diffraction peaks gradually moved toward smaller angles, which can be attributed to the difference in ionic radius. The slight translation results from methylammonium with smaller ionic radius (2.70 Å) replaced by formamidinium with relatively larger ionic radius (2.79 Å) that expands the crystal lattice. The XRD observation implies that we can easily substitute the cations through the facile drop-casting technique and exchange reaction occurs on the top surface of $MAPbI_3$ thin film. The $FAPbI_3$ (black phase) was reported to have a cubic structure, while $MAPbI_3$ has a tetragonal structure, and at room temperature, the difference lies in a slight rotation of the lead iodide octahedron. However, these crystal structures are fundamentally similar, so they would be likely to support intermixing and facile conversion between them without much lattice stress.[13] The exchange reaction on the $MAPbI_3$ thin film was further confirmed from the FTIR spectrum for the $FA_xMA_{1-x}PbI_3$ perovskite. Figure 6 reveals the following spectral features and peak positions for the formamidinium; C=N stretching vibrations from MA coordinated to FA at 1680 cm^{-1}; N–H stretching in the range about 1620 cm^{-1}–3440 cm^{-1}; C–H stretching both located at 2920 cm^{-1}.

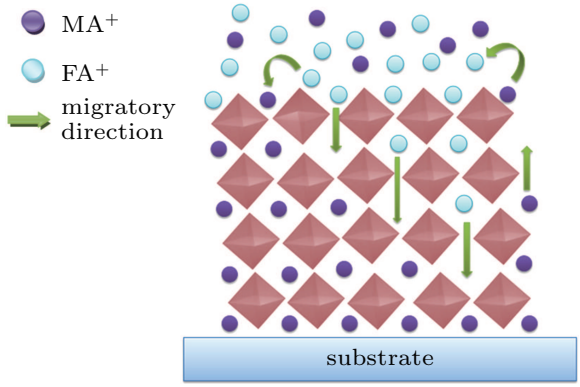


Fig. 3. (color online) Illustration of the cation exchange process of the FA^+ and MA^+ during annealing.

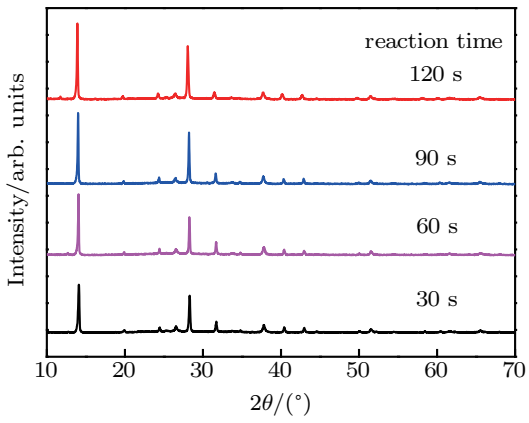


Fig. 4. (color online) X-ray diffraction patterns of $FA_xMA_{1-x}PbI_3$ with different reaction times based on"drop-casting"technology (10 mg/ml FAI isopropanol solution).

The detection of C=N in the perovskite layer guarantees the successful substitution of MA^+ with FA^+ through this "drop-casting" method. According to the relationship between interplanar spacing and FA^+ content shown in the literature,[20] the FA_x MA_{1-x} PbI_3 perovskite can be identified as $MAPbI_3$, $FA_{0.03}$ $MA_{0.97}$ PbI_3, $FA_{0.1}$ $MA_{0.9}$ PbI_3 , $FA_{0.15}$ $MA_{0.85}$ PbI_3, $FA_{0.2}$ $MA_{0.8}$ PbI_3, corresponding to FAI concentrations of 0 mg/ml, 2 mg/ml, 5 mg/ml, 10 mg/ml, and 15 mg/ml, respectively.

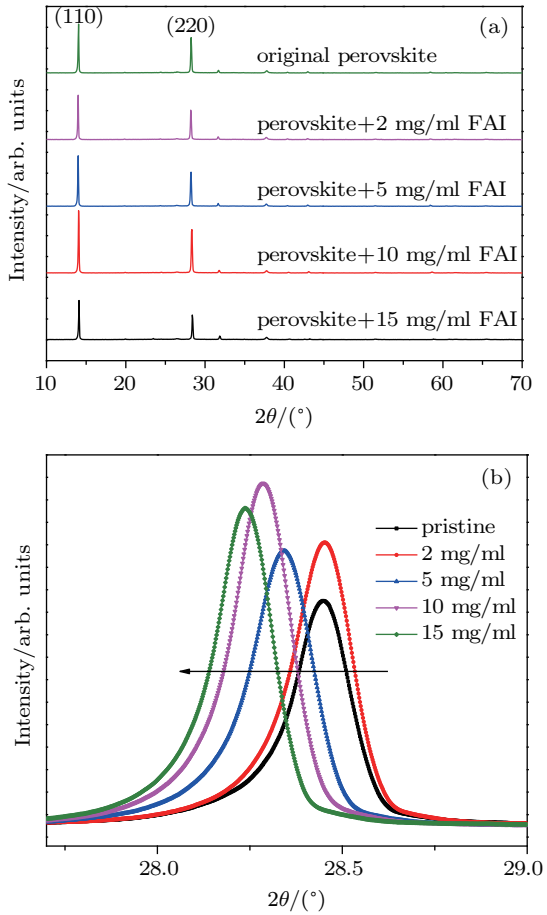


Fig. 5. (color online) (a) X-ray diffraction patterns of $FA_xMA_{1-x}PbI_3$ with different reaction concentrations of FAI, and (b) magnified x-ray diffractions in the range of 28°–29°.

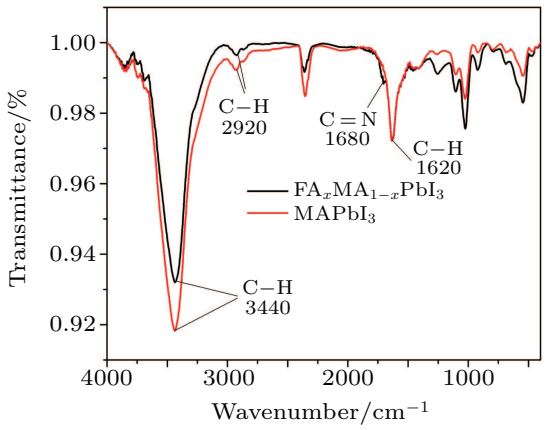


Fig. 6. (color online) FTIR spectra of the $FA_xMA_{1-x}PbI_3$. C=N stretching and bending, showing that the perovskite film includes formamidinium cation.

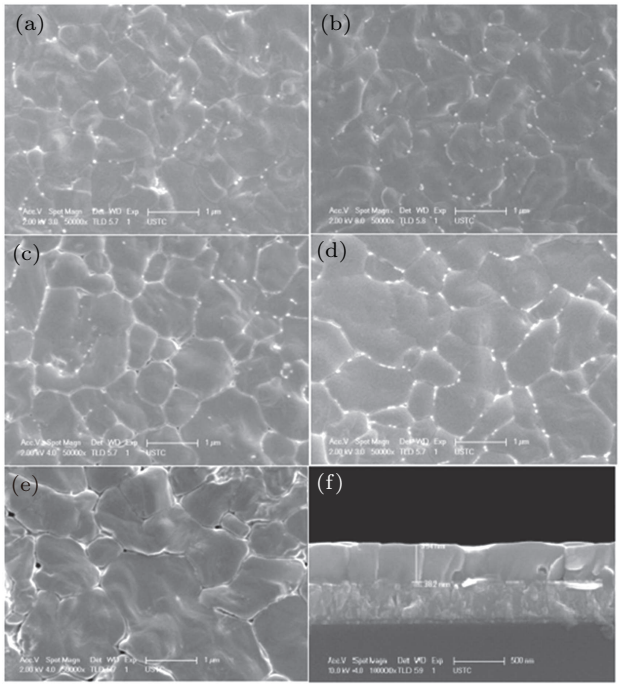


Fig. 7. ((a)–(e)) Surface topographic SEM images of $FA_xMA_{1-x}PbI_3$ films with different reaction concentrations of FAI (0 mg/ml, 2 mg/ml, 5 mg/ml, 10 mg/ml, 15 mg/ml), and (f) cross-sectional SEM image of perovskite film $FA_{0.15}MA_{0.85}PbI_3$ reaction with 10 mg/ml FAI solution.

Surface morphologies of the $FA_xMA_{1-x}PbI_3$ perovskite films reacting with different concentration FAI solutions are analyzed by SEM (Fig. 7). Dense and high-quality crystalline films of $MAPbI_3$ (Fig. 7(a)) are observed after the annealing process, which manifests that the "one-step" method and planar structure are suitable for the preparation of perovskite film. With the FAI solution concentration increasing from 2 mg/ml to 15 mg/ml, the density of the film first increases then decreases and reaches an optimal morphology with 10 mg/ml ($x = 0.15$) shown in Fig. 7(d), whereas the grain size continuously increases as shown in Figs. 7(b)–7(e). With the concentration of FAI solution further increasing to 15 mg/ml, pinholes and cracks appear (Fig. 7(e)), which not only reduces the effective light absorption but also leads to short-circuiting in the ultimate devices. The differences in the surface morphology among perovskite films on the planar substrates will distinctly affect the device performance. Furthermore, the cross-section SEM images (Fig. 7(f)) reveal that the perovskite film $FA_{0.15}MA_{0.85}PbI_3$ owns a grain lateral size equal to film thickness of 400 nm, which implies that the photo generated charges could reach the corresponding electrode interface without passing through several grain boundaries, which act as recombination centers and reduce device performance. The charge carriers can efficiently transport within one single grain without losing many charges. The cross-section surface of perovskite film unteated by FAI solution is rough as shown in Fig. 8. Although the SEM images (Figs. 7(b)–7(d)) show that the grains tend to be larger in size with the increase of concentration, the crystallite sizes in the films are significantly different, as illustrated in Fig. 7(e), while the grains grow to a similar size in the films with low FAI concentration (Figs. 7(a) and 7(b)). As is well known, the ideal grain growth can be approximately expressed by the following quadratic: $d_1^2 - d_2^2 = k_1 \exp(-Q/RT)$, where d_1 and d_2 are the initial and final grain size, k_1 is a constant, and T, R, and Q are the absolute temperature, radius of the grain sphere, and activation energy for boundary mobility, respectively. Given k_1, Q, T and the preparation conditions are almost the same, the homogeneity of the grain size depends on activation energy for the boundary mobility.[21] The formula reveals that larger activation energy results in more homogeneous grain size. The isopropanol solution of FAI may reduce the activation energy of the boundary mobility, making the new grains grow into different size ones.

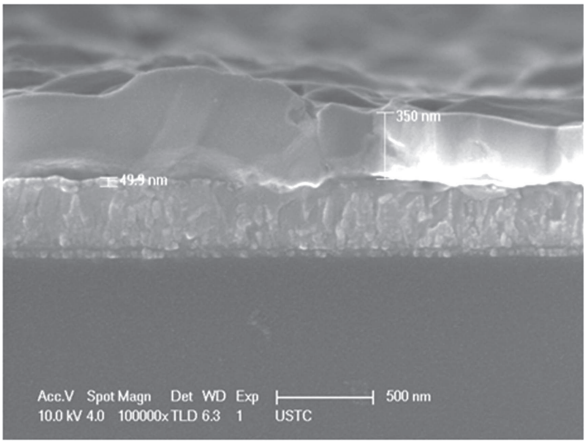


Fig. 8. Cross-sectional SEM image of perovskite (MAPbI3) film untreated by FAI solution.

To find out the variations of optical properties in the cation hybrid perovskite ($FA_xMA_{1-x}PbI_3$), we measure the UV-visible absorption spectra of $FA_xMA_{1-x}PbI_3$ thin film as shown in Fig. 9(a). A tiny shift of the absorption band edge to longer wavelength is observed with the increase of concentration. As the onset absorption wavelength moves toward the infrared direction, the energy band gap decreases gradually. It should be noted that this "red-shift" originates from the differences in spin orbital coupling between Pb and I, and also in simultaneous structural transition. The Pb–I bond length in PbI_6 octahedron in $FAPbI_3$ with the tetragonal structure is in a range of 3.169 Å–3.181 Å, whereas in cubic structure $MAPbI_3$, the Pb-I bond length varies from 3.156 Å to 3.213 Å.[22] The energy band gap value is obtained from the intersection between the linear extrapolation of the edge of the absorption band and the horizontal axis. The specific calculation tangent chart is shown in Fig. 10. The variations in the energy band gap value are shown in Fig. 9(b), and the range of the energy band gap (range from 1.51 eV–1.54 eV) is consistent with that reported in the literature.[23]

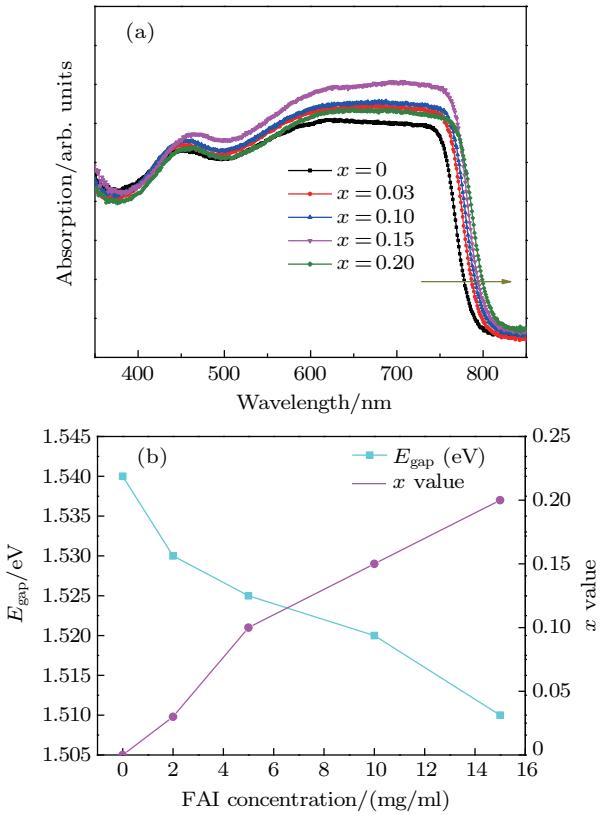


Fig. 9. (color online) (a) UV-visible absorption spectra of $FA_xMA_{1-x}PbI_3$ films and (b) variations of energy band gap and x value of $FA_xMA_{1-x}PbI_3$ films with different concentrations of FAI (all films have the same reaction time).

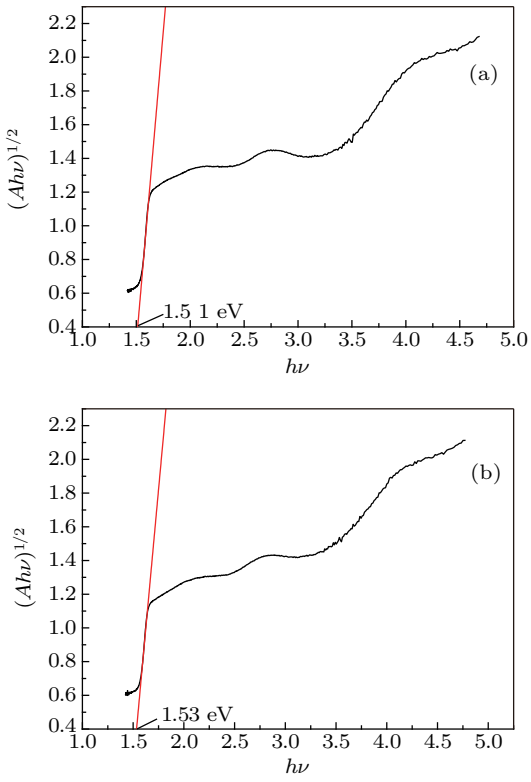


Fig. 10. (color online) (a) $h\nu$–$(Ah\nu)^{1/2}$ curve of perovskite $FA_{0.2}MA_{0.8}PbI_3$ reaction with FAI with 15 mg/ml (tangent point: $h\nu = 1.570$; $Ah\nu^{1/2} = 0.881$; slope = 8.031); (b) $h\nu$–$(Ah\nu)^{1/2}$ curve of perovskite $FA_{0.03}MA_{0.97}PbI_3$ reaction with FAI with 2 mg/ml (tangent point: $h\nu = 1.602$; $Ah\nu^{1/2} = 0.848$; slope = 6.558).

Based on the one-step method with a planar structure, perovskite solar cells with an FTO/TiO_2/$FA_xMA_{1-x}PbI_3$/spiro-OMeTAD/Ag planar structure are fabricated. The photovoltaic performance of perovskite solar cells is shown in Table 1. The characteristic J–V curves are shown in Fig. 11(a). With the FAI solution concentration increasing from 2 mg/ml to 15 mg/ml, the J_{sc} of the device first increases then decreases and reaches a maximum value of 20.53 mA·cm^{-2} for 10 mg/ml, whereas the Voc reaches a minimum value for 10 mg/ml mainly due to the lower photon energy stemming from the narrowing of energy band gap. Besides, when the FAI concentration increases from 2 mg/ml to 10 mg/ml for $FA_xMA_{1-x}PbI_3$ perovskite film, large and well connected grains are observed without any pinholes (Figs. 7(b)–7(d)), which is consistent with the device PCE improvement. With the concentration further increasing to 15 mg/ml, pinholes and cracks appear (Fig. 7(e)), which explains the declining of the device J_{sc} and PCE. A large number of cracks and pinholes existing in the film lead to massive recombination between electrons and holes and eventually the PCE of the device decreases. Therefore, the optimum reaction concentration of FAI is determined to be 10 mg/ml ($x = 0.15$), in which the PCE is improved from 12.59% to 14.3%.

The photoelectric conversion characteristics of the fabricated devices with different reaction concentrations are further investigated by measuring their IPCE as revealed in Fig. 11(b). The values of J_{sc} measured from the J–V curves match well with those integrated from the IPCE, which are 17.28 mA·cm^{-2} and 18.87 mA·cm^{-2} for $x = 0$ and $x = 0.15$, respectively. The best device also shows a very broad IPCE plateau of over 80% between 430 nm and 620 nm as shown in Fig. 11(b). The IPCEs in the short wavelength region ($\sim$ 350 nm) are similar based on the two devices. This is mainly because the light-harvesting efficiency is nearly saturated due to the high absorbance of perovskite in the short wavelength region.[24] The photo-to-electron quantum efficiencies of the wavelengths ranging from 450 nm to 770 nm are significantly different, and there is a distinct increase for the device with $FA_{0.15}MA_{0.85}PbI_3$ perovskite film. The denser perovskite film and enhanced light-harvesting capability have naturally been considered as being due to one reason. Besides, the sample with $FA_{0.15}MA_{0.85}PbI_3$ shows wider absorption edges at around 815 nm with broad absorption over the entire visible region, which is in agreement with the previous UV-vis result. Moreover, histograms of current density and efficiency of device with different FAI concentrations are shown in Fig. 12, indicating that the average efficiency and average current density are more than 13.5% and 19.4 mA·cm^{-2}, each with a narrow size distribution. It shows a truth that current density and efficiency of the cell will be greatly improved through "drop-casting" technology with 10-mg/ml FAI solution ($x = 0.15$).

Table 1. Photovoltaic parameters of cells with different-parameter solar cells fabricated.

FAI concentration/(mg/ml)	x value	J_{sc}/(mA·cm^{-2})	V_{oc}/V	FF/%	PCE/%
0	0	18.78	0.99	67.91	12.59
2	0.03	18.18	0.99	72.77	13.13
5	0.10	18.92	0.95	74.66	13.37
10	0.15	20.53	0.93	74.59	14.30
15	0.20	19.28	0.96	72.75	13.40

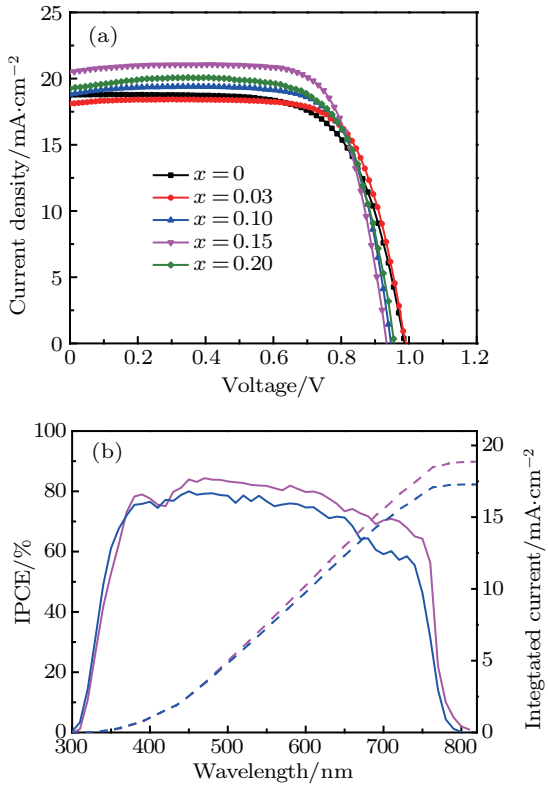


Fig. 11. (color online) (a) J–V curves for perovskite cell with different reaction concentrations, measured by reverse scans in voltage steps of 10 mV and with 40-ms delay times under AM 1.5G illumination. (b) IPCE spectra of the perovskite devices with different reaction concentrations. The integrated photocurrents (dash lines) are calculated from the overlap integral of the IPCE spectra.

To study the charge extraction properties of the TiO_2 and perovskite layer with different "drop-casting" concentrations, PL analyses are conducted respectively. The $FA_xMA_{1-x}PbI_3$ is a highly luminescent material, thus the quenching of its PL intensity is used as a measure of the ability of the perovskite layer to extract the charges. Figure 13 gives the PL spectra of the perovskite ($FA_xMA_{1-x}PbI_3$) deposited on compacted TiO_2/nonconductive glass substrates. Owing to the insulating substrate, the PL spectra also could reflect the quality of individual perovskite films. An obvious emission peak gradually moves toward the long wavelength with the increase of concentration, which also indicates a decreasing trend of band gap. This result is consistent with the previous conclusion which was drawn from UV-vis analysis. As shown in Fig. 13, the (cp) TiO_2 layer presents a great potential in almost completely extracting the electrons from the perovskite with $x = 0.15$ because the PL intensity is minimum in Fig. 13. It also shows that perovskite film and (cp) TiO_2 layer substrate are contacted closely at the interface, which is an important factor for obtaining the better performance of perovskite solar cell.

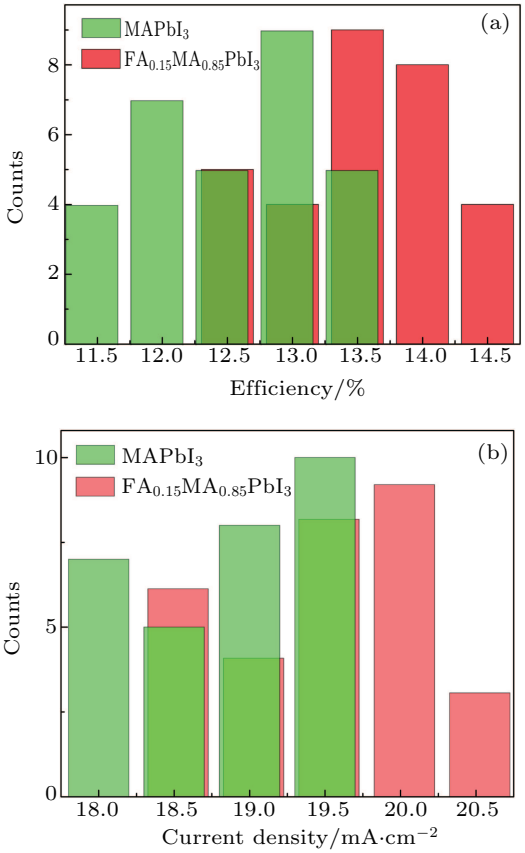


Fig. 12. (color online) Histograms of efficiency (a) and current density (b) of device for different FA^+ content values.

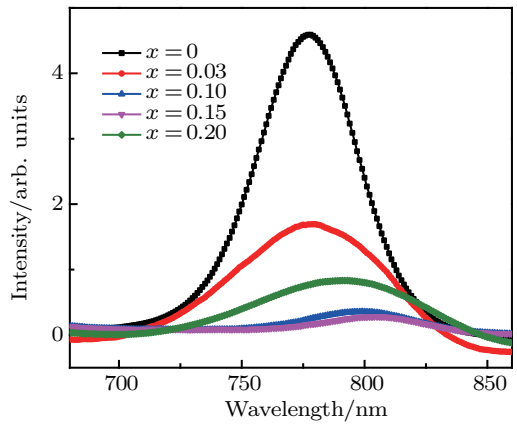


Fig. 13. (color online) PL spectra of different FA^+ concentration perovskite films deposited on compacted TiO_2/nonconductive glass substrates.

The *J*–*V* hysteretic behavior investigated by varying the scan direction (forward scan is defined as a measure from the short circuit to the open circuit and reverse scan is a measure from the open circuit to the short circuit). As can be seen in Fig. 14, with FA^+ added into perovskite solar cell, the hysteresis value decreases. The phenomenon that the increasing of the FA component can obviously reduce the hysteresis has also been reported in the literature.[18] Kim and Park elucidated that the degree of hysteresis depends strongly on perovskite crystal size and mesoporous TiO_2 layer.[25] Considering the fact that the thickness of mesoporous TiO_2 layer is constant, minor hysteresis can be attributed to the higher purity and larger size of crystal (discussed in Fig. 7), but the details need further studying.

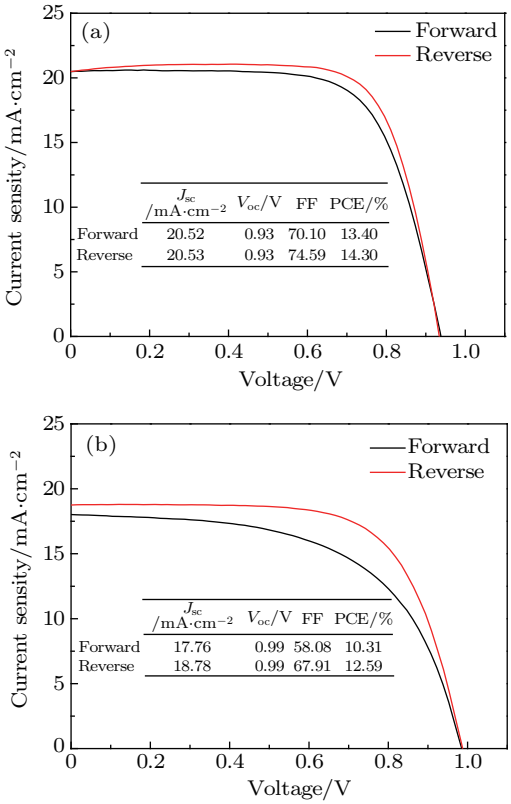


Fig. 14. (color online) Photovoltaic performances as a function of scan direction. (a) The best device based on $FA_xMA_{1-x}PbI_3$ ($x = 0.15$) perovskite, (b) original perovskite ($MAPbI_3$) cell device without FA^+ component.

4. Conclusions

In this work, a facile and cost-effective method is employed to fabricate cation hybrid perovskite ($MA_{1-x}FA_xPbI_3$) films and the devices with $MA_{0.85}FA_{0.15}PbI_3$ perovskite film with the highest 14.3% PCE under standard conditions (AM 1.5G radiation, 100 mW·cm^{-2}). Furthermore, these results unveil that the optimal exchange reaction concentration of FAI isopropanol solvent is 10 mg/ml in this "drop-casting" technique and the crystallinity has no significant difference with reaction time longer than 90 seconds. Hence, these results provide important progress towards the solution-processing in the realizing of low-cost and highly efficient perovskite solar cells.

References

[1] Im J H, Lee C R, Lee J W, Park S W and Park N G 2011 *Nanoscale* **3** 4088
[2] Zhou H, Shi Y, Dong Q, Zhang H and Xing Y 2014 *J. Phys. Chem. Lett.* **5** 3241
[3] Xing G, Mathews N, Sun S, Lim S S and Lam Y M 2013 *Science* **342** 344
[4] Stranks S D, Eperon G E, Grancini G, Menelaou C and Alcocer M J 2013 *Science* **342** 341
[5] Yao X, Ding Y L, Zhang X D and Zhao Y 2015 *Acta Phys. Sin.* **64** 38805 (in Chinese)
[6] Chai L and Zhong M 2016 *Acta Phys. Sin.* **65** 237902 (in Chinese)
[7] Woon S Y, Jun H N, Nam J J, Young C K, Seungchan R, Jangwon S and Sang S 2015 *Sci. Rep.* **10** 1126
[8] Yan W, Rao H, Wei C, Liu Z and Bian Z 2017 *Nano Energy* **35** 62
[9] Jian Q, Chandran H T, Cheng Y H, Tsang S W and Lo M F 2016 *Org. Electron.* **38** 144
[10] Zhou Y, Yang M, Pang S, Zhu K and Padture N P 2016 *J. Am. Chem. Soc.* **138** 5535
[11] Zhou Z, Pang S, Ji F, Zhang B and Cui G 2016 *Chem. Commun.* **52** 3828
[12] Pellet N, Teuscher J, Maier J, Grätzel M 2015 *Chem. Mater.* **27** 2181
[13] Eperon G E, Beck C E and Snaith H J 2015 *Materials Horizons* **3** 63
[14] Chuang C L, Chen C Y, Chiang C H and Wu C G 2017 *Inorganic Chemistry Frontiers*
[15] Jian Q, Chandran H T, Cheng Y H, Tsang S W and Lo M F 2016 *Org. Electron.* **38** 144
[16] He X, Guo P F, Wu J H, Tu Y G and Lan Z 2017 *Solar Energy* **157** 853
[17] Zhao B G, Zhu L, Zhao Y L, Yang Y and Song J 2016 *J. Mater. Sci. Mater. Electron.* **27** 10869
[18] Ji F, Wang L, Pang S, Gao P and Xu H 2016 *J. Mater. Chem. A* **4** 14437
[19] Lee J, Seol D, Cho A and Park N 2014 *Adv. Mater.* **26** 4991
[20] Slimi B, Mollar M, Assaker B I, Kriaa I, Chtourou R and Mari B 2016 *Energy Procedia* **102** 87
[21] Chuang C L, Chen C Y, Chiang C H and Wu C G 2017 *Inorg. Chem. Frontiers* **4** 850
[22] Stoumpos C C, Malliakas C D and Kanatzidis M G 2013 *Inorg. Chem.* **52** 9019
[23] Yang Z, Chueh C C, Liang P W, Crump M and Lin F 2016 *Nano Energy* **22** 328
[24] Yang H, Zhu J, Yong D, Chen S and Zhang C 2016 *Acs Appl. Mater. Interfaces* **8** 8162
[25] Kim H S and Park N G 2014 *J. Phys. Chem. Lett.* **5** 2927